scientific reports

Check for updates

OPEN

Commonalities in gene expression and methylation changes across two rat models of acquired epilepsy

Benton S. Purnell[1,6], Junguk Hur[2,6], David Ruskin[3], Madhuvika M. Murugan[1], Fabio Tescarollo[1], Riddhimaa Sinha[1], Nikhil Ramavenkat[1], Susan A. Masino[3], Jonathan D. Geiger[2] & Detlev Boison[1,4,5]✉

Changes in DNA methylation and gene expression play a major role in the epileptogenic process that turns a healthy brain into an epileptic brain. Previous investigations have focused either on changes in the transcriptome or epigenome, but rarely on both. The goal of this combined transcriptomic and epigenomic investigation was to identify shared and distinct changes in gene expression and DNA methylation in two widely used, but mechanistically distinct, rat models of temporal lobe epilepsy: intrahippocampal electrical kindling and systemic kainic acid induced epilepsy. RNA sequencing and reduced-representation bisulfite sequencing were used to assess differences in gene expression and DNA methylation. We found gene expression and methylation changes specific to each model, and genes with altered expression ($n = 71$) or methylation ($n = 94$) in the same direction in both models. Remarkably, there was no overlap between these genes that were either altered in their expression or methylation in the same direction in both models. Furthermore, there was no consistent relationship between the direction of methylation and expression changes in either model. These observations indicate that transcriptomic and epigenetic changes during epileptogenesis are distinct processes, which is of importance for the discovery of disease-modifying therapeutics that act on a transcriptomic or epigenomic level.

Keywords Epilepsy, Epileptogenesis, Epigenetics, DNA methylation, Gene expression

The epilepsies are a highly prevalent set of neurological conditions characterized by spontaneous recurrent seizures[1,2]. Currently, there are over 20 anti-seizure medications (ASMs) in common use, with additional ASMs being made available with some regularity[3,4]. Despite the abundance of ASMs, rates of refractory epilepsy have remained stable, at approximately one-third, for over four decades[5]. As a result, it seems unlikely that additional traditional ASMs will substantively improve rates of seizure control. Furthermore, many who are able to attain seizure freedom with traditional pharmacological therapy must contend with the side effects of these medications, which may detrimentally affect their personal and professional lives[6,7]. Lastly, conventional ASMs do not have disease-modifying effects and, as such, their capacity to suppress seizures persists only as long as the drug is present in the blood of the patient[8,9]. There is now a concerted effort to identify treatments that directly interfere with epileptogenesis, the process that transforms a healthy brain into an epileptic brain, rather than identifying novel ASMs[10–12]. The development of therapeutic interventions that are effective in a higher proportion of patients, have fewer side effects, and have persistent disease-modifying effects necessitates a better understanding of the epileptogenic process, which is multifactorial and involves changes in both gene expression and epigenetic signatures[12–16]. Unbiased screens for the changes in gene expression and methylation underlying epileptogenesis are promising tools in this enterprise[17–19].

The methylation hypothesis of epileptogenesis, first formulated by Kobow et al., is based on findings from human epilepsy and preclinical models of temporal lobe epilepsy and implies that acquired DNA methylation changes play a major role in the progression of epileptogenesis[13,20–23]. An early study associated increased methylation of the *reelin* promoter with granule cell dispersion in human temporal lobe epilepsy[22].

[1]Department of Neurosurgery, Robert Wood Johnson Medical School, Rutgers University, Piscataway, NJ 08854, USA. [2]Department of Biomedical Sciences, University of North Dakota, School of Medicine and Health Sciences, Grand Forks, ND 58202, USA. [3]Department of Psychology and Neuroscience, Trinity College, Hartford, CT 06106, USA. [4]Brain Health Institute, Rutgers University, Piscataway, NJ 08854, USA. [5]Rutgers Cancer Institute, Rutgers University, New Brunswick, NJ 08904, USA. [6]These authors contributed equally this work: Benton Purnell and Junguk Hur. ✉email: detlev.boison@rutgers.edu

Subsequent sequencing approaches have demonstrated that maladaptive DNA methylation is a major driver of the epileptogenic process[23–26] and that human epilepsy, as well as acute seizure models, are characterized by differential DNA methylation patterns or by increased DNA methyltransferase activity[23,25,26]. Key findings from these studies demonstrate a predominant increase of DNA methylation in a pilocarpine-induced rat model of chronic epilepsy with methylation changes mostly confined to gene bodies[24]. Interestingly, this study also identified methylation changes that did not correspond with gene expression changes, which included differential gene expression for several epigenetic enzymes and binding motifs for key transcriptional activators (*Nfkb*, *Kat2a*, *Zzz3*, *Gtf2b*, *p300*) and repressors (*Nrsf*, *Suz12*)[24]. In contrast, a study by Miller-Delaney et al.l showed mostly DNA hypomethylation in promoter regions following an experimental status epilepticus[26] indicating that DNA hypomethylation might be a consequence of prolonged seizures, whereas DNA hypermethylation is associated with chronic epilepsy, consistent with the identification of promoter hypermethylation in human resected hippocampal tissue from patients with temporal lobe epilepsy undergoing resective surgery[25]. In our own study performed in the rat systemic kainic acid model of epilepsy we identified genes with increased methylation status during epileptogenesis and then determined those whose methylation status could be normalized by transient antiepileptogenic adenosine treatment. Among these genes we found several polymerases, such as *PolD*, and DNA-interacting zinc finger proteins[23]. In addition to methylation changes described above, more recent work has identified changes in DNA hydroxymethylation (5hmC) in association with epilepsy, exercise, and behavioral training[27–29]. Interestingly, the bulk DNA levels of 5hmC were reduced in human epileptic hippocampus as well as in the kainic acid rat model[27]. Based on 5-hmC hMeDIP-sequencing data, hypo-hydroxymethylation of intergenic regions was associated with several epilepsy-related genes, such as *Gal*, *SV2*, and *Kcnj11* and hyper-hydroxymethylation of intergenic regions was associated with *Gad65*, *TLR4*, and *Bdnf* genes[27]. Although the use of more advanced methylation arrays such as MeDIP and hMeDIP sequencing approaches allow the distinction between 5mC and 5hmC sites, in contrast to non-specific whole-genome bisulfite sequencing, these and other pioneering studies used bulk tissue-level approaches, which lacked cellular specificity. Single-cell transcriptomics performed on human epileptic brain tissue has identified specific pro-epileptogenic neuronal subtypes and inflammatory mechanisms as key drivers of epilepsy[30,31]. Novel approaches such as single-cell ATAC-seq and single-cell methyl-seq can map chromatin accessibility and DNA methylation patterns at the single-cell level and are expected to lead to more refined insights into acquired DNA methylation changes during the epileptogenic process.

The goal of this investigation was to identify shared and distinct changes in gene expression and methylation in two mechanistically different rat models of temporal lobe epilepsy. We chose the electrical hippocampal kindling and systemic kainic acid rat models of epilepsy. In the hippocampal kindling model, seizures are experimentally induced and a fully kindled epileptic state is created by periodic, unilateral, sub-convulsive electrical stimulation of the hippocampus[32,33]. In the systemic kainic acid model, acute chemoconvulsant-induced status epilepticus precipitates subsequent spontaneous recurrent seizures[34]. The epileptogenic process in the systemic kainic acid model is characterized by more profound cytoarchitectural reorganization, inflammatory processes, and glial activation than the hippocampal kindling model[35]. These models were selected because of their widespread use and because, though ostensibly modeling temporal lobe epilepsy, their etiologies are different in substantial ways.

Here, we pursued a dual approach to assess both bulk gene expression changes as well as DNA methylation changes at the level of the CpG site from hippocampal specimens derived from rats with and without the development of temporal lobe epilepsy, in two etiologically different model systems. We focused on hits that are common between both models as well as a pairwise comparison analysis for differences between the two models. Gene ontology enrichment analysis was performed on both the shared and distinguishing changes in methylation and expression between models.

Results

The goal of this investigation was to identify changes in gene expression and methylation associated with epileptogenesis that are shared and distinct in two rat models of temporal lobe epilepsy (Fig. 1A). Our approach was to use RNA sequencing to assess differences in gene expression and reduced-representation bisulfite sequencing (RRBS) to assess differences in gene methylation in the rat hippocampal kindling and systemic kainic acid models.

Specifically, the models used to induce epileptogenesis were intra-hippocampal electrical kindling and systemic kainic acid-induced status epilepticus. The four conditions for tissue extraction and analysis were: (1, Kindling 3ClassV) implanted with intrahippocampal stimulation electrodes, kindled with repeated stimulation, and sacrificed after their third evoked Racine Class V seizure; (2, Kindling Sham) implanted with kindling electrodes, but not stimulated; (3, Kainic Acid 3ClassV) implanted with intrahippocampal recording electrodes, injected with kainic acid, and sacrificed after their third spontaneous Racine Class V seizure; and (4, Kainic Acid Sham) implanted with recording electrodes, but injected with saline.

Similarities and differences between the hippocampal kindling and systemic Kainic acid rat models of epileptogenesis

Robust seizures were observed following repeated hippocampal stimulation in the kindling model (Fig. 1B) and spontaneously following a latent period after chemoconvulsant-induced status epilepticus in the systemic kainic acid model (Fig. 1C). The timetable utilized in this study resulted in a latency from the start of epileptogenesis to the third Class V seizure (characterized by forelimb clonus, rearing, and falling on a modified Racine scale) that was comparable between models (Supplementary Fig. S1A; $t(11) = 0.95$, $p = 0.362$). As anticipated, anatomical examination of the hippocampus in a subset of animals revealed effectively normal cytoarchitecture in the epileptic kindled brain (Fig. 1D-E), whereas the KA-induced epileptic brain was characterized by profound

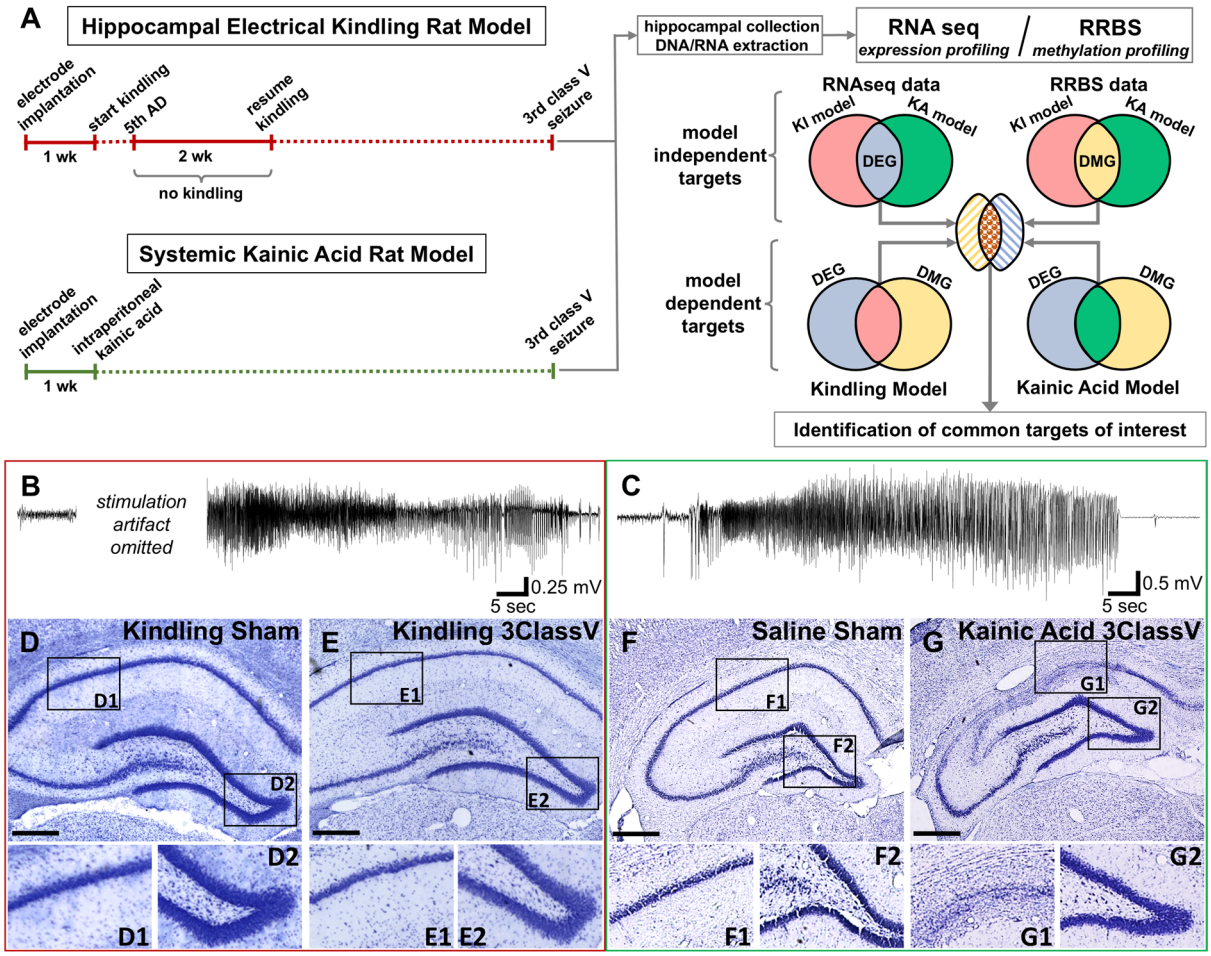

Fig. 1. Approach for the identification of model-dependent and model-independent epileptogenesis targets and electrographic/histological features of the models. (**A**) Schematic diagram depicting the experimental timeline of two well-established animal models of epileptogenesis: the hippocampal electrical kindling model (KI; AD, afterdischarge) and the systemic kainic acid model (KA). Hippocampi were dissected from rats in these epilepsy models after their third Racine Class V (Class V) seizure or from sham rats. RNA and DNA were extracted from the tissue and submitted for RNA sequencing and reduced-representation bisulfite sequencing (RRBS), respectively. Data were analyzed to identify model-independent and model-dependent changes in gene expression and DNA methylation. Cortical EEG traces of representative Racine Class V seizures in the intrahippocampal electrical kindling (**B**) and post systemic kainic acid-induced status epilepticus (contributed equally) rat models of epileptogenesis. Both traces are 90 s in duration. Seizures in the kindling model were evoked by a 10 s tetanic electrical pulse; the stimulation and consequent artifact have been omitted to avoid confusion with endogenous epileptiform discharges. Seizures in the kainic acid model were spontaneous. Representative micrographs of Nissl-stained hippocampal tissue from a sham-operated rat (**D**), a hippocampally kindled rat (**E**), a sham rat treated with saline (**F**), and a rat treated with systemic kainic acid (**G**). Insets depict 2x magnified images of CA1 (D1, E1, F1, G1) and the dentate gyrus (D2, E2, F2, G2).

histopathology, most notably a severe loss of CA1 neurons (Fig. 1F-G). Thus, both models are histopathologically different, consistent with the neuroinflammatory etiology of the KA model[35].

Gene expression analysis using RNA-seq in kindling and systemic kainic acid rat models

An average of 56 million single-end reads per sample were generated by RNA-seq (Supplementary Fig. S1B). All samples had high-quality single-end RNA-seq reads, with an average of 99% of reads passing the quality filtering process, which removes adapter contamination, poly-N sequences, and reads with quality scores < 30 (Supplementary Fig. S1B). Approximately 68% of the total reads uniquely aligned to exons in the rn6 reference rat genome[36]. In both the kindling (Fig. 2A) and kainic acid (Fig. 2B) models, the experimental 3ClassV and Sham groups showed clear separation on principal component analysis (PCA) plots. DESeq2 identified 3,625 differentially expressed genes (DEG) between the Sham and 3ClassV groups in the kindling model and 349

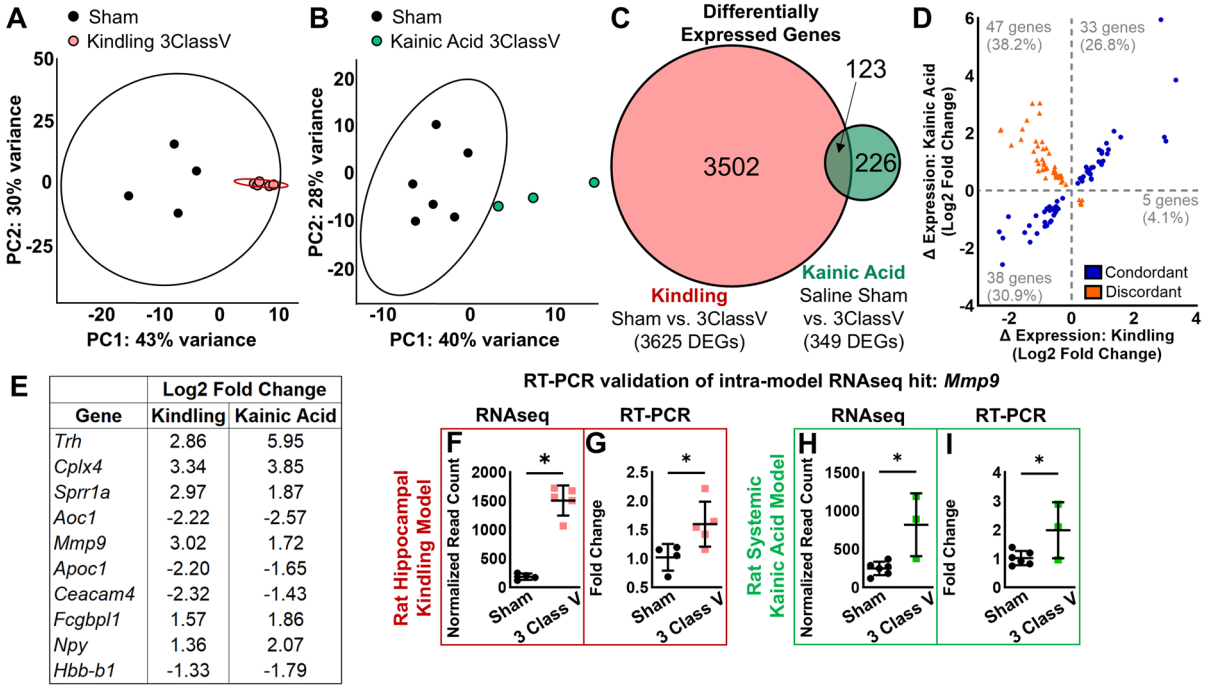

Gene	Log2 Fold Change	
	Kindling	Kainic Acid
Trh	2.86	5.95
Cplx4	3.34	3.85
Sprr1a	2.97	1.87
Aoc1	-2.22	-2.57
Mmp9	3.02	1.72
Apoc1	-2.20	-1.65
Ceacam4	-2.32	-1.43
Fcgbpl1	1.57	1.86
Npy	1.36	2.07
Hbb-b1	-1.33	-1.79

Fig. 2. The effects of hippocampal kindling and systemic kainic acid on gene expression. Principal component analysis (PCA) was performed to examine the similarity of expression profiles in the RNA-seq data from the kindling (**A**; sham, black; fully kindled, red) and the kainic acid (**B**; sham, black; kainic acid, green) models of epileptogenesis ($n = 3–6$ rats). (**C**) Venn diagram of differentially expressed genes (DEGs) in the kindling model (red, 3,625 genes), in the kainic acid model (green, 349 genes), and in both models (123 genes). (**D**) Scatter plot depicting genes that were significantly altered in expression in the kainic acid model (y-axis) and the kindling model (x-axis). Concordantly affected genes that were altered in the same direction in both models are colored blue, and discordantly affected genes are orange. (**E**) List of the 10 genes most strongly altered in their expression in a concordant direction in both models. Values for each gene represent Log2 fold change (FC) from the control group. RNA-seq data from *Mmp9*, one of the most altered genes in its expression pattern between models, is depicted in dot plots (**F**, **H**) and validated via reverse transcription polymerase chain reaction (RT-PCR) (**G**, **I**). Data are mean ± SD, $n = 3–6$. *, $p < 0.05$ unpaired two-tailed t-test. Data are plotted as mean ± SD. *, $p < 0.05$ unpaired two-tailed t-test.

DEGs in the kainic acid model (Fig. 2C). A total of 123 DEGs were shared between the two models (Fig. 2C). Approximately 58% of the shared DEGs (71) showed concordant directionality of gene expression changes between the models (Fig. 2D; blue genes in upper-right and lower-left quadrants) and represent genes of interest (Fig. 2E, Supplementary Table 1) commonly regulated in the same direction in two etiologically different epilepsy models. To statistically evaluate the observed overlaps, we conducted permutation-based significance testing. The overlap between the DEG sets from the kindling and kainic acid models, while modest in absolute count ($n = 123$), was highly significant compared to random expectation (Fig. 2C; $Z = 10.19$, $p < 0.001$), indicating shared gene regulation across models.

As a further quality control measure, we used RT-PCR to validate the expression levels of *Mmp9*, one of the genes most differentially expressed during epileptogenesis in both models (Fig. 2G, I), to corroborate the results of the RNA-seq data (Fig. 2F, H). In the kindling model, unpaired two-tailed *t*-tests revealed an increase in *Mmp9* expression both in the RNA-seq and the RT-PCR assessments (Fig. 2F-G; RNA-seq, $t(7) = 9.86$, $p < 0.001$; RT-PCR, $t(7) = 2.59$, $p = 0.036$). Similar increases in *Mmp9* expression were observed using RNA-seq and RT-PCR in the systemic kainic acid model (Fig. 2H-I; RNA-seq, $t(7) = 3.49$, $p = 0.010$; RT-PCR, $t(7) = 2.44$, $p = 0.045$).

To address the potential influence of altered cell-type heterogeneity on gene expression between models, we performed a cell-type deconvolution analysis on our RNA-Seq data using CIBERSORT[37]. Our analysis, based on a mouse hippocampus-derived class-level reference from the Allen Brain Cell Atlas (12 classes; top 100 marker genes per class), mapped to rat genes, and observed non-zero fraction values for 8 classes in our dataset (Supplementary Fig. S2). Kruskal-Wallis tests identified overall group differences in broad neuronal (glutamatergic and GABAergic) and glial classes, the oligodendrocyte-lineage class did not show a significant difference across groups (Supplementary Table S3). Post-hoc testing suggested that these differences were primarily driven by the kindling model, whereas no corresponding Sham versus 3ClassV differences were observed within the kainic acid model (Supplementary Table S4). Detailed test statistics and adjusted P-values

are provided in Supplementary Table S3. Because deconvolution provides computationally inferred cell-type fractions rather than direct measurements, these results are interpreted as a composition check and should be validated in future studies, ideally using single-cell or single-nucleus assays.

DNA methylation analysis using reduced representation bisulfite sequencing (RRBS) in kindling and systemic Kainic acid rat models

To identify genes and pathways epigenetically associated with epileptogenesis, we next examined genome-wide DNA methylation changes using RRBS profiling. Over 94% of the reads were high quality, and the bisulfite conversion rate was approximately 98% across all samples (Supplementary Fig. S1C). CpG sites on X and Y chromosomes were excluded, resulting in a total of 1.6 million CpG sites identified for differential methylation analysis. Unlike the RNA-Seq data (Fig. 2A-B), the methylation profiling data did not show a clear separation between Sham and 3ClassV groups in their respective PCA plots (kindling model Fig. 3A, kainic acid model Fig. 3B). *methylKit* identified significant differences in CpG site methylation (adjusted p-value < 0.01 and methylation difference > 25%). Differentially methylated CpGs were distributed across promoters, exons, introns, and intergenic regions without substantial differences between models or conditions (Supplementary Fig. S3A-D). When mapped at the gene-level, 1,150 and 1,380 differentially methylated genes (DMGs) were observed in the kindling and systemic kainic acid models, respectively (Fig. 3C). Approximately one-third of the DMGs (352) were commonly differentially methylated between the two models; however, only 94 genes, approximately 27% of the 352 common DMGs, show concordant directionality (Fig. 3D, Supplementary Table 2; blue genes in upper-right and lower-left quadrants). The 10 genes with the largest concordant changes in methylation between the two models are shown (Fig. 3E). To statistically evaluate the observed overlaps, we conducted permutation-based significance testing. The overlap between the DMG sets from the kindling and kainic acid models was statistically significant (Fig. 3C; $Z = 36.69$, $p < 0.001$).

We also assessed region-level methylation using a 1-kb tiling-based differentially methylated region (DMR) analysis (*methylKit*) with gene annotation. Most DMR-associated genes overlapped the DMG sets across comparisons: Kainic Acid-Sham (110/151), Kindling-Kainic Acid (153/216), Kindling-Sham (96/166),

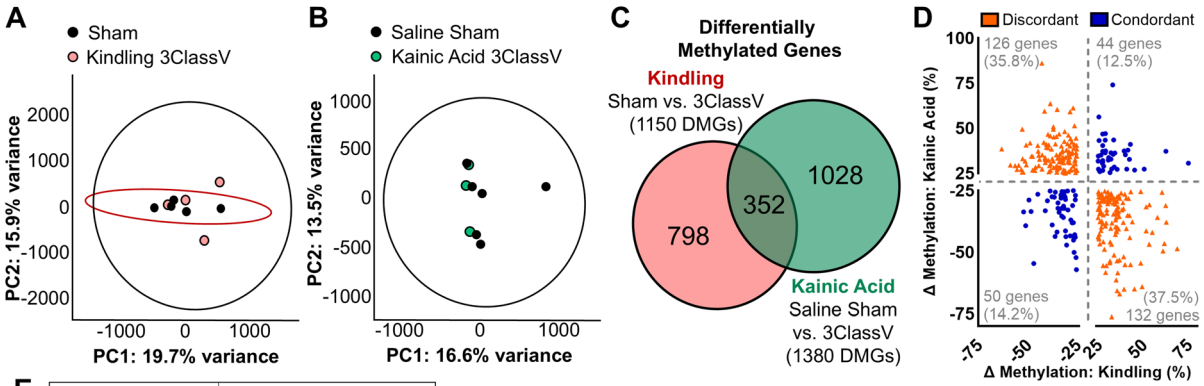

E

	Methylation % change	
Gene	Kindling	Kainic Acid
Zfp281	33.09	73.98
Vps29	75.15	30.54
Da2-19	-46.89	-54.65
Plcxd3	62.67	37.22
AABR07071482.2	-50.98	-39.32
AABR07017189.1	-52.01	-33.67
Eif4g2	42.89	41.00
Zfp385b	-25.28	-57.16
AABR07036442.1	-48.22	-33.55
AABR07034574.1	25.47	56.21

Fig. 3. The effects of hippocampal kindling and systemic kainic acid on gene methylation. Principal component analysis (PCA) was performed to examine the similarity of methylation profiles in the RRBS data from the kindling (**A**; sham, black; fully kindled, red) and the kainic acid (**B**; sham, black; kainic acid, green) models of epileptogenesis ($n = 3$–6 rats). (**C**) Venn diagram of differentially methylated genes (DMGs) in the kindling model (red, 1,150 genes), in the kainic acid model (green, 1,380 genes), and in both models (352 genes). (**D**) Scatter plot depicting genes that were significantly altered in methylation in the kainic acid model (y-axis) and in the kindling model (x-axis). Concordantly affected genes that were altered in the same direction in both models are colored blue, and discordantly affected genes are orange. (**E**) List of the 10 genes most strongly altered in their methylation in a concordant direction in both models. Values for each gene represent the percentage change from the control group.

and Sham-Sham (53/95), corresponding to ~56–73% overlap, about two-thirds overall. Venn diagrams for each comparison are shown in Supplementary Fig. S3E-F. DMR-only genes were modest in numbers (41–70) compared with the larger DMG-only sets (e.g., Kainic Acid-Sham: 1,270; Kindling-Kainic Acid: 1,539; Kindling-Sham: 1,054; Sham-Sham: 898), consistent with broader gene-level coverage by CpG-aggregated DMGs. Given this substantial overlap and gene-centric downstream integration with expression, we focused subsequent analyses on DMGs.

Pairwise comparisons between models

To explore the shared and divergent biological changes between the models in more detail, we performed all possible pairwise differential gene expression analyses. The number of DEGs identified in each comparison is summarized in Supplementary Fig. S4A. Our analysis revealed minimal gene expression differences between the two sham groups, indicating a low level of inherent variability between the naive states of the models. In contrast, the comparison between the experimental groups that had undergone epileptogenesis in each model revealed a significant number of DEGs. A four-way Venn diagram (Supplementary Fig. S4B) demonstrated that the overlap between the DEG sets from the kindling and kainic acid models was limited, suggesting that the two models induce largely distinct transcriptional changes. The directionality of these changes was further visualized in an alluvial plot (Supplementary Fig. S4C). Subsequent GO enrichment analysis of the DEG sets highlighted that the two models drive substantially different biological processes (Fig. 4). For instance, while both models showed altered immune-related pathways, the specific enriched terms were distinct, suggesting different mechanisms of neuroinflammation. A full hierarchical clustering heatmap showing the relative gene expression levels across samples for all DEGs has been created to enable visualization of the data at the level of specific genes for each replicate (Supplementary Fig. S5). These findings indicate that while both models lead to the development of epilepsy, they do so through divergent molecular and cellular pathways.

Complementing these expression results, pairwise methylation analyses yielded broadly similar DMG counts across all four comparisons (Supplementary Fig. S4D): Kindling-Sham (1,269), Kainic Acid-Sham (1,532), Kindling-Kainic Acid (1,794; the largest), and Sham-Sham (1,031). Unlike the RNA-seq results, substantial differences were already evident between the two sham groups, indicating baseline methylomic divergence between models. The within-model and between-model epileptogenic comparisons showed comparably large methylation remodeling. The four-way Venn and alluvial summaries (Supplementary Fig. S4E-F) indicate modest cross-comparison sharing with substantial comparison-specific DMG components.

Overlap analysis between DMGs and DEGs

To understand the relationship between epigenetic regulation and transcriptomic changes, we examined the overlap between DMGs and DEGs in both epileptogenesis models. In the kindling model, 181 genes were shared between the DMGs and DEGs, while 34 genes were shared in the systemic kainic acid model (Fig. 5A). Figure 5B-C illustrates the shared DEGs and DMGs with differential expression levels (log2FC) and methylation levels (delta-methylation%). To statistically evaluate the observed overlaps, we conducted permutation-based significance testing. The overlap between DEGs and DMGs was statistically significant for the kainic acid model (Fig. 5A; $Z = 3.04$, $p = 0.0035$), but not for the kindling model (Fig. 5A; $Z = -0.65$, $p = 0.752$). These shared genes were divided into four categories based on the directional changes in DNA methylation and gene expression: "Hypo-Down" for the hypomethylated and downregulated genes, "Hypo-Up" for the hypomethylated and upregulated genes, "Hyper-Down" for the hypermethylated and downregulated genes, and "Hyper-Up" for the hypermethylated and upregulated genes. While the kindling model included 43% in the "Hyper-Down" and "Hypo-Up" categories, 70.5% of the shared genes in the systemic kainic acid model were included in these two groups.

Genes that are differentially methylated and differentially expressed, independent of the model

Finally, the overlap between the 123 model-independent differentially expressed genes and the 352 model-independent differentially methylated genes was determined (Fig. 5D) and revealed five new genes that were differentially methylated and expressed in both models: *Fcgbpl1*, *Loxhd1*, *Nedd9*, *Ptpre*, and *Adcy4* (Fig. 5D), all of which were increased in expression in both models except for *Adcy4*, which was increased in the kindling model and decreased in the kainic acid model. (Fig. 5E-N; *Fcgbpl1*, kindling $t(7) = 3.11$. $p = 0.017$, kainic acid $t(7) = 4.54$, $p = 0.003$; *Loxhd1*, kindling $t(7) = 2.92$, $p = 0.022$, kainic acid $t(7) = 4.69$, $p = 0.002$; *Nedd9*, kindling $t(7) = 4.21$, $p = 0.004$, kainic acid $t(7) = 3.16$, $p = 0.016$; *Ptpre*, kindling $t(7) = 4.71$, $p = 0.002$, kainic acid $t(7) = 2.57$, $p = 0.037$; *Adcy4*, kindling $t(7) = 4.82$, $p = 0.002$, kainic acid $t(7) = 5.71$, $p < 0.001$).

We further examined the CpG site-specific methylation of the five genes that were commonly differentially methylated and expressed in both the kindling and the systemic kainic acid models. Supplementary Fig. S6 illustrates the relative locations and methylation levels of the measured CpG sites of these genes across the two models. Interestingly, those CpG sites that were deemed significantly differentially methylated, indicated by pink boxes, were commonly differentially methylated, but their directions of differential methylation was opposite between models. For example, the differential CpG site in *Fcgbpl1* showed hyper-methylation in the 3ClassV group of the kindling model, while the same CpG site in the kainic acid model showed significant hypo-methylation.

Discussion

Improving the rates of refractory epilepsy beyond those afforded by current antiseizure medications and the development of disease-modifying treatments capable of preventing epileptogenesis, both AES/NINDS

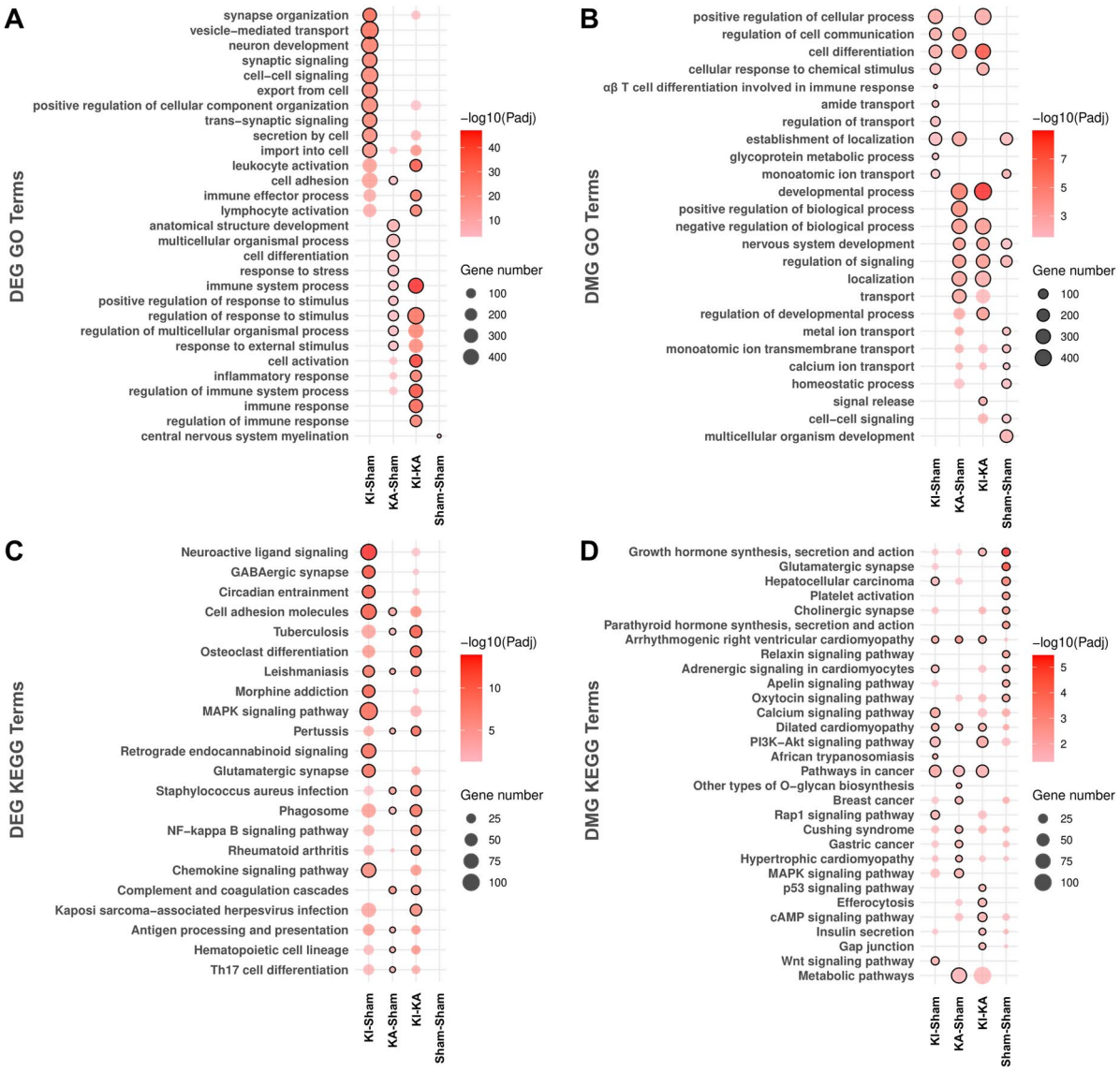

Fig. 4. Functional enrichment analysis of differentially methylated and expressed genes. Enrichment analysis was performed using the Gene Ontology (GO)[86] and Kyoto Encyclopedia of Genes and Genomes (KEGG)[87] classification systems. Significant GO terms were passed through the DAVID Gene Functional Classification Tool[88]. The ten most strongly altered categories among differentially expressed genes (DEG; A, C) and differentially methylated genes (DMG; B, D) for the GO (**A-B**) and KEGG (**C-D**) classification systems are plotted as a dot. Comparisons are made between kindled and sham rats (KI-Sham), kainic acid-treated and sham rats (KA-Sham), kindled and kainic acid-treated rats (KI-KA), and the sham groups in each model (Sham-Sham). Dot size corresponds to the number of affected genes in the category and color indicates log10 (adjusted *p* value).

Epilepsy Research Benchmarks[10,11], will likely necessitate the development of interventions that target novel mechanisms. For logistical and ethical reasons, the toolset available for identifying target mechanisms is stronger in experimental animal models than in naturally occurring human epilepsy. Unfortunately, insights derived from any animal model are limited in clinical significance by issues of generalizability. Even insights that can be leveraged to prevent seizures or epileptogenesis in the model from which they are derived are of limited usefulness if the mechanism is idiosyncratic to that model. In this investigation, we proceeded with the supposition that changes in gene regulation would be more likely to represent a generalizable feature of the epilepsies and would be more useful in the development of treatments if those changes are (A) generalizable between differing animal models (i.e. systemic kainic acid and intrahippocampal electrical kindling in rats) and (B) manifested both in changes in gene expression as well as DNA methylation.

We predicted that the kainic acid model would be associated with more differentially expressed and methylated genes because (A) the seizures in this model are spontaneous, not evoked like in the kindling model, (B) the kainic acid model causes more profound cytoarchitectural reorganization than the kindling model

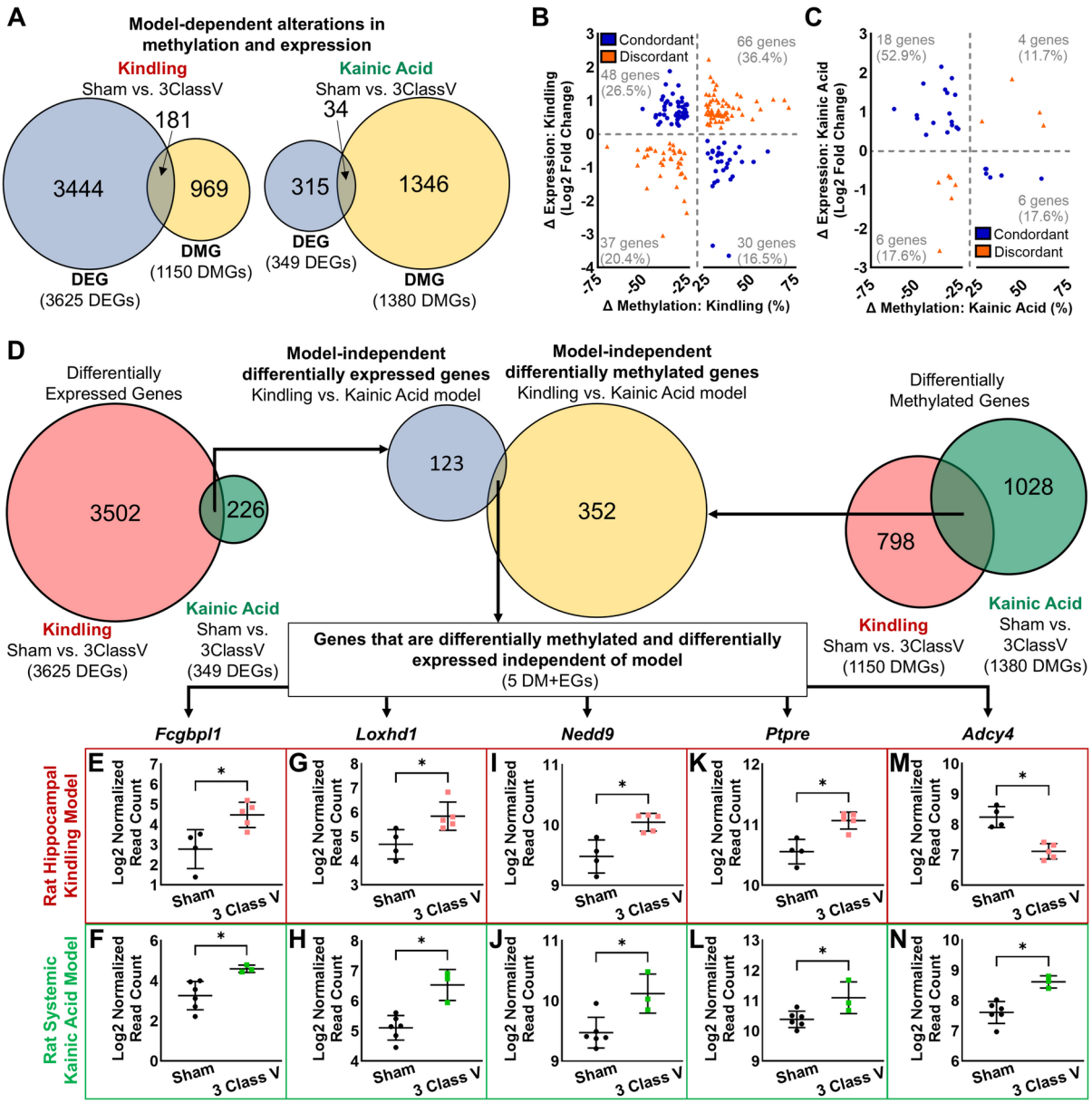

Fig. 5. Model-dependent and model-independent effects on gene expression and methylation. (**A**) Venn diagrams of differentially expressed genes (DEG, blue), differentially methylated genes (DMG, yellow), or both differentially methylated and expressed genes in rats having undergone 3 Racine Class V seizures (3ClassV; Kindling: 3625 DEG, 1150 DMG, 181 both; Kainic acid: 349 DEG, 1380 DMG, 34 both). Scatter plots depicting genes that were significantly altered in expression (y-axis) and methylation (x-axis) in the kindling model (**B**) and the kainic acid model (**C**). Concordantly affected genes that were altered in the conventionally expected direction in expression and methylation are colored blue, and discordantly affected genes are orange. (**D**) Venn diagrams depicting the identification of genes that were differentially expressed in both rat models (123, left), genes that were differentially methylated in both rat models (352, right), and genes that were differentially methylated and differentially expressed in both rat models (5, center; GM + EGs). Dot plots depicting the effect of epileptogenesis in the rat electrical kindling model (upper row) and the rat systemic kainic acid model (lower row) as assessed by RNA-seq on *Fcgbpl1* (B-C), *Loxhd1* (D-E), *Nedd9* (F-G), *Ptpre* (HI), and *Adcy4* (J-K). $n = 3$–6, data are plotted as mean ± SD. *, $p < 0.05$ unpaired two-tailed t-test.

(Fig. 1D-G), and (C) the kainic acid model is precipitated by severe status epilepticus that has no parallel in the kindling model. In contrast to our expectations, the kainic acid model resulted in only slightly more differentially methylated genes (+20%, Fig. 3C) and drastically fewer differentially expressed genes (−90.4%, Fig. 2C) than the kindling model.

Why is the kindling model associated with greater changes in gene expression? This finding is intriguing and surprising, given the factors listed above that facially make the kindling model appear phenotypically milder.

The progressive aggravation of epileptiform discharges following stimulations in the kindling model necessitates progressive changes in network excitability. This reprogramming of excitability might have a more profound effect on gene expression than the lesional sclerotic damage caused by kainic acid exposure. Alternatively, the increased expression in the kindling model may be the result of the brain area sampled. RNAseq analysis was performed on the left hippocampus, which is where the stimulation electrode was implanted in the kindling model but has no special significance in the kainic acid model. Lastly, the larger change in gene expression seen in the kindling model may be the result of greater variability in the gene expression profile within the kainic acid model (Fig. 2A-B). High within-group variability is commonly observed in models of traumatic brain injury and stroke[38,39], likely due to stochastic differences in the physiological reaction of the animal to the injurious event. Similar stochastic differences in the physiological reaction to status epilepticus may increase variability in the kainic acid model. Indeed, in the systemic kainic acid rodent models it is common practice to titrate kainic acid dose based on the response of each animal to ensure comparable status epilepticus severity between animals[39].

Matrix metalloproteinase-9, the enzyme that *Mmp9* encodes, is upregulated by albumin exposure through activation of the mitogen-activated protein kinase (MAPK) signaling pathway[40]. The role of *Mmp9* in dendritic spine morphology, long-term potentiation, and seizure-induced cytotoxicity has previously been linked to the mechanisms of epileptogenesis[41–43]. In this dataset, *Mmp9* was strongly differentially regulated in its expression between the two models. Considering existing interest in *Mmp9* during epileptogenesis, the changes in its expression observed in the RNA-seq data were confirmed using RT-PCR (Fig. 2F-I).

Why is the kainic acid model associated with greater changes in DNA methylation? Kainic acid exposure generates substantial astrogliosis, inflammation, cell death, and activation of astrocytes and microglia[44–46]. Electrical kindling has a milder effect on these processes, which may mediate the increased methylation seen in the kainic acid model. Additional experimentation will be necessary to evaluate the role of these processes in the epileptogenesis-induced alterations in DNA methylation.

We identified only five genes that were differentially methylated and expressed in both models; however, they might have generalizable relevance to epileptogenesis and warrant further discussion (Fig. 5D-N). The gene *Fcgbpl1* codes IgGFc-binding protein. Though the function of IgGFc-binding protein is not well understood, it binds to immunoglobulin G and may serve as a substrate for its sequestration[47,48]. Immunoglobulin G is the most common antibody in blood plasma[49]. Epilepsy increases immunoglobulin G leakage into the brain[50,51], which is associated with neurodegeneration[50]. Our interpretation is that blood-brain barrier dysfunction due to repeated seizures increases immunoglobulin G extravasation into the brain, which causes compensatory changes in Fcgbp expression and methylation. *Nedd9* encodes the protein neural precursor cell expressed developmentally down-regulated protein 9 and has been implicated in epileptogenesis by prior investigations in humans[52] and in experimental models[53,54]. Reports using the mouse intrahippocampal kainic acid model found *Nedd9* to be overexpressed at 12 and 24 h following the injection[54]. Our data suggest that this increase in *Nedd9* expression is sustained chronically and not idiosyncratic to chemoconvulsant models. *Ptpre* encodes receptor-type tyrosine-protein phosphatase epsilon, an enzyme capable of dephosphorylating the tyrosine residues of insulin, JAK2, and Kv2.1 receptors[55–58]. *Ptpre* knockout mice display increased phosphorylation of voltage-gated potassium channels, decreased activity of these channels, and increased neuronal excitability[59]. The beneficial effect of maintaining adequate potassium channel dephosphorylation on neuronal excitability indicates that the increase in *Ptpre* expression observed across models in this investigation may be an adaptive compensatory response. *Adcy4* codes the enzyme adenylyl cyclase type 4, which catalyzes the formation of cyclic adenosine monophosphate (cAMP). cAMP decreases GABA receptor currents and increases glutamate receptor currents[60,61]. Accordingly, increased cAMP increases neuronal excitability and epileptiform activity[62]. Alterations in *Adcy4* expression have been observed in another unbiased screen in a rodent model[63]. A caveat of this approach is that while differentially methylated genes were associated with concordant gene expression changes across models, the directionality of the observed DNA methylation changes was different across models. This could be due to our analysis of global DNA methylation changes in each gene driving the overall directionality of the observed change, whereas individual DNA methylation sites might drive gene expression changes.

Principal component analysis (PCA) was performed to examine the similarity of expression profiles in the RNA-seq data (Fig. 2A-B) and methylation profiles in the RRBS data (Fig. 3A-B). Large and consistent differences in gene expression profiles were found in both models. In contrast, the RRBS data did not indicate consistent differences in gene methylation patterns in either model.

It is possible that differences in the death or proliferation of specific cell types between the kindling and kainic acid models could have driven some of the observed changes in gene expression or methylation. The bulk tissue approach used in this investigation does not enable the examination of changes in gene expression or methylation within specific cell types. However, since different cell types generally have different expression profiles, it is possible to draw inferences regarding the balance of cell types in the samples from each group. We employed the CIBERSORT computational approach to cell type deconvolution using the RNAseq data[37]. Kindled rats had an increased fraction of infered astrocytes and glutamatergic cells, but a reduced fraction of immune cells, relative to the sham group. The increase in astrocytes in kindled rats is consistent with epileptogenesis-associated astrogliosis, though it is surprising that there was no enrichment in astrocytic markers in kainic acid treated rats. The increase in glutamatergic cell markers is suggestive of increased excitatory signaling and is consistent with prior transcriptomic examinations of hippocampal kindling in rats[64]. The reduction in immune markers in kindled rats is generally in keeping with the paradigm that kindling, unlike chemoconvulsant models, does not induce widespread neuroinflamation[44–46]. Critically, deconvolution approaches such as this infer cell-type fractions based on typical cell-type selective transcription patterns, which may be altered by epileptogenesis. These observations should be validated in future studies, ideally using single-cell or single-nucleus assays.

The central insights of this investigation are: (1) In these disparate models, epileptogenesis had a more consistent and robust effect on gene expression than methylation. (2) Though some of the alterations in gene expression seen in epileptogenesis may be the result of altered gene methylation, much of the epileptogenesis-associated gene expression changes are not mediated by a change in gene methylation. If a preponderance of altered gene expression was the result of altered methylation, broader or more consistent differences in methylation patterns between sham and experimental groups would be expected. (3) Though changes in gene expression and methylation between each model were largely non-overlapping (Figs. 2C and 3C), the overlap was greater than that which would be predicted by chance, suggesting shared mechanisms of epileptogenesis. (4) Finally, while within-model overlaps between differentially methylated and expressed genes were modest in number, a greater proportion of the overlapping genes in the kainic acid model exhibited concordant directional changes, suggesting a possible tendency toward more coordinated transcriptional and epigenetic regulation in this model that warrants further investigation. Given the small gene count, this observation should be interpreted cautiously and considered hypothesis-generating rather than definitive.

Several limitations should be considered. The directionality of methylation changes (hypo- vs. hypermethylation) is governed by the average change of multiple methylation sites within each gene. This contrasts with individual methylation sites driving gene expression changes, which could override the average change in gene methylation. This gene-level aggregation approach may under-represent localized regulatory effects at functionally important regions, such as promoters, and should be considered as a limitation of the current analysis. In addition, our data were generated using standard bisulfite-based RRBS, which does not allow the distinction between 5mC and 5hmC; thus, increases in 5mC in conjunction with decreases in 5hmC might lead to an apparent 'neutral' methylation outcome. Finally, RRBS has restricted, enzyme-biased genomic coverage and may miss methylation changes outside CpG-enriched regions; genome-wide profiling (for example, whole-genome bisulfite sequencing) could identify additional alterations.

Despite these limitations, the findings from our cross-model comparisons lead us to the following overall conclusion: In the development of novel treatments for the epilepsies, promising gene targets identified in one model should be systematically investigated in other models. Moreover, lack of generalizability (contradictory results emerging from different models) must not be confused with failures of replicability (contradictory results emerging from the same model). Interesting context for this conclusion is provided by the successes of the Epilepsy Therapy Screening Program (formerly the Anticonvulsant Screening Program). This program also uses a combination of two mechanistically distinct electrical and chemoconvulsant models[65]. If generalizability between models is as limited as our results suggest, examinations of genetic and epigenetic factors in multiple models is expected to be more insightful than if any one model were used.

Materials and methods

Animals and ethical approval

All procedures and protocols used in this study were approved by the Institutional Animal Care and Use Committee (IACUC) of Rutgers University in accordance with the international guidelines set by the Association for Assessment and Accreditation of Laboratory Animal Care (AAALAC). Experimentation, analysis, and reporting were conducted in compliance with ARRIVE guidelines[66]. Care was taken to use the minimum number of animals possible and to minimize their pain and distress. All animals were housed under a 12:12 light/dark cycle (lights on at 6 am). Food (5053, PicoLab) and water were available *ad libitum*. In both epilepsy models, rats were randomly assigned to experimental groups. Animals were excluded from the analysis only if they failed to develop three Class V seizures.

Systemic Kainic acid rat model

Adult, male, Sprague-Dawley rats of ~ 170 g (001, Charles River Laboratories) were surgically instrumented with a bipolar recording electrode in the left hippocampus (from bregma; AP: −4.2 mm, ML: −3.0, DV: −3.3) under isoflurane anesthesia (1.5% in O_2). The head of the animal was fixed in a Kopf stereotactic frame, and a midline incision was made in the scalp after administration of a local anesthetic (bupivacaine, 0.15 ml, 2.5 mg/ml) and a systemic analgesic (Ethiqa XR, 0.65 mg/kg). After at least seven days of surgical recovery, these rats received incremental kainic acid (KA) injections at regular intervals to induce status epilepticus with comparable severity between animals (35–55 mg/kg total) or sham saline injections of comparable volume. In both the kainic acid and kindling models, behavioral seizures were scored using a modified Racine scale (0, 'wet dog' shakes; I, behavioral arrest; II, facial automatisms, head bobbing, eye twitching; III, forelimb clonus; IV, forelimb clonus and rearing; V, forelimb clonus, rearing, and falling)[67]. Only animals that experienced three hours of convulsive, Racine Class ≥ IV seizures were included in the investigation. Animals were continuously monitored via video/EEG starting two weeks after status epilepticus until they experienced three Racine Class V seizures. The EEG signal was relayed via a 6-channel cable (363–363, Plastics One) from the animal to a commutator (SL6C/SB, Plastics One) and then to an amplifier (FE232, AD Instruments). The amplified signal was then digitized (PowerLab; AD Instruments) and recorded on a PC. EEG files were analyzed by an observer blinded to the treatment condition of the animal. EEG seizures were defined as periods of high-frequency, high-amplitude, rhythmic discharges with an evolving pattern that lasted at least 5 s. Euthanasia and tissue collection were performed within 24 h of the last Class V seizure.

Intrahippocampal electrical kindling rat model

Adult, male, Sprague-Dawley rats of ~ 280 g were used in the kindling protocol. The surgery was conducted under isoflurane anesthesia (1.5% in O_2). The head of the animal was fixed in a Kopf stereotactic frame, and a midline incision was made in the scalp after administration of a local anesthetic and a systemic analgesic (bupivacaine and Ethiqa as above). Two burr holes were drilled in the skull (from bregma; AP: +3.0, ML: +2.0

and AP: −7.0, ML: −2.0) and threaded with EEG screw electrodes (E363-20, Plastics One). A third burr hole was drilled over the left hemisphere, and an insulated, stainless steel, bipolar twisted pair electrode (E363/2-2TW/SPC, Plastics One) was implanted into the hippocampus (from bregma; AP: −5.0, ML: −5.0, DV: −7.5) and fixed in place with dental cement. Prior to the surgery, the tips of the stimulating electrodes were separated by ~0.5 mm, and the insulation was removed from the last ~0.5 mm of wire. The socket ends of the EEG screw electrodes and hippocampal stimulation electrodes were fixed in a 6-channel polyethylene pedestal (MS363-6, Plastics One). The electrodes, wires, and the underside of the pedestal were insulated and adhered to the skull using dental cement.

One week following surgical instrumentation, the animals were kindled by twice-daily electrical stimulation via the hippocampal electrode. Kindling stimulations were separated by at least one hour. The 10 s, 50 Hz, 5 V, biphasic, 1 ms pulse duration, square wave stimulation was provided by a Grass S-88 stimulator. To better match the timescale of the systemic kainic acid model, in which Racine grade V seizures appear after a protracted latent phase, a two-week break in the kindling stimulation paradigm was given after the fifth stimulation that generated hippocampal afterdischarges. Discontinuation of kindling is a common approach to study epileptogenic mechanisms, whereby interruption of kindling is not associated with epilepsy progression[68]. Rats were fully kindled after their 3rd Racine grade 5 seizure. Euthanasia and tissue collection were performed 24 h after the last seizure.

Hippocampal tissue extraction and processing

The rats in this study were euthanized via decapitation, and whole hippocampi from each animal were surgically dissected fresh, flash-frozen in liquid N_2, and stored at −80 °C before being processed for deep sequencing analysis. Qiagen's AllPrep DNA/RNA Mini Kit (Product ID: 80204) was used to extract RNA and DNA from the left hippocampus of each animal. The left hippocampus was used because that was the hemisphere in which the stimulation electrode was placed in the kindling model and consequently the brain area containing the epileptogenic zone in that model.

Total RNA isolated from the individual sample was evaluated using a TapeStation system (Agilent). Samples with a minimum RNA integrity number of 8 were processed with the NEBNext Ultra II RNA Library Prep Kit for Illumina (New England Biolabs) to construct the sequencing library. The RNA-sequencing library was sequenced with a single-end read length of 110 bases using an Illumina NovaSeq platform (Illumina) by the Rutgers University Genomics Center blinded to the experimental condition of the animal.

The total genomic DNA was processed for reduced representation bisulfite sequencing (RRBS) by the Rutgers University Genomics Center using previously described methods[69]. Briefly, genomic DNA quantity was measured using a Qubit fluorometer (ThermoFisher Scientific) and assessed using TapeStation (Agilent). Genomic DNA was digested with *Msp1* restriction enzyme and purified using phenol: chloroform extraction and ethanol precipitation. Following *Msp1* digestion, genomic DNA underwent blunt-end digestion, phosphorylation, and ligation of adapters with methylated cytosines. Ligated fragments, processed for size selection using agarose gel electrophoresis, were bisulfite converted, amplified by PCR, and then cleaned using AMPure XP beads (Beckman Coulter Life Sciences). Libraries were established using Qubit fluorometric quantification (ThermoFisher Scientific), analyzed using a TapeStation system (Agilent), and then sequenced on an Illumina NovaSeq platform (Illumina) with a single-end read length of 110 bases by the Rutgers University Genomics Center.

RNA-Seq and RRBS data processing

The quality of the RNA-Seq data was examined using the *FastQC* v0.11.9 quality control tool[70]. Raw sequencing reads were cleaned using *Trimmomatic* v0.39[71] to remove and trim reads with adapters, poly-N sequences, or sequences with low Phred quality scores (< 30)[72]. Cleaned reads were mapped to the rat reference genome rn6 using *HISAT2* v2.2.1[73]. Genes with zero expression across samples were omitted from differential expression analysis. Mapped reads were assigned to unique genomic features using *featureCounts*[74]. Principal Component Analysis (PCA) was performed to gain insights into the association between samples and visualized using the fviz_pca_ind function of factoextra with addEllipses = TRUE to display 95% confidence regions. Differentially expressed genes (DEGs) were identified using the *DESeq2* R package with a significance cutoff of < 0.05 adjusted *p*-value[75] between the 3ClassV and Sham groups in each of the kainic acid and kindling models.

Quality control assessment of RRBS data was completed using *FastQC* v0.11.9[70]. Raw sequencing reads were cleaned using *Trim Galore* v0.6.4, to remove and trim reads with adapter contamination and sequences with a low Phred quality score (< 30)[72]. Cleaned reads were mapped to the in-silico bisulfite-converted rat reference genome rn6 using *Bismark* v0.23.0 and *Bowtie2* v2.3.5.1[76,77]. CpG sites on X and Y chromosomes were excluded. PCA was performed on the most variable 10% of the measured CpG sites. To count uniquely mapped reads and to assess changes in methylation between each site, *methylKit* v1.8.1 was used[78] (Fig. 3, Supplementary Fig. S3E-H). Differentially methylated CpGs (DMCs) were defined as a ≥ 25% difference in cytosine methylation levels between sites with an adjusted *p*-value < 0.01 between 3ClassV and Sham groups in the kainic acid and kindling models. These DMCs were then aggregated into differentially methylated genes (DMGs) based on unique gene identifiers. DMCs were annotated with the *genomation* R package[79] (gene-based and CpG-island features), and their genomic context (promoter, exon, intron, intergenic) was summarized. Annotation of murine CpG islands was obtained from the University of California, Santa Cruz, Genome Browser Gateway. The gene annotation was obtained from Ensembl and NCBI gene databases[80]. In addition to single-site DMCs, we identified differentially methylated regions (DMRs) by tiling the genome into 1-kb windows and performing a similar statistical analysis to detect broader regions of methylation change between groups. Overlap between DMR-associated genes and DMGs was quantified and visualized with Venn diagrams, generated by VennDetail v1.23.0 (https://github.com/hurlab/VennDetail).

To perform a more comprehensive comparison of gene expression changes, we also performed all pairwise differential gene expression analyses across the four experimental groups (Kindling Sham, Kindling 3ClassV, Kainic Acid Sham, and Kainic Acid 3ClassV). Overlap between the resulting DEG sets was visualized using a four-way Venn diagram. To compare the direction of gene expression changes, we generated an Alluvial plot. Furthermore, to identify the biological pathways affected in each comparison, we conducted Gene Ontology (GO) enrichment analysis using our in-house R package, richR (https://github.com/hurlab/richR/). The analysis focused on the GO Biological Process terms, and a merged list of significantly enriched terms was generated from each DEG set.

To assess the statistical significance of gene set overlaps, including those between differentially expressed genes (DEGs), differentially methylated genes (DMGs), and cross-omics overlaps across epilepsy models, we performed a random permutation test. For each comparison, we randomly selected gene sets from the total gene pool, matching the sizes of the two sets being tested (for example, Kindling vs. Kainic Acid DEGs or DEG vs. DMG sets). This process was repeated 10,000 times to generate a null distribution of expected overlaps by chance. The significance of the observed overlap was then determined by calculating a Z-score and p-value, comparing the observed overlap to the mean and standard deviation of the null distribution.

Cell-type composition analysis

To infer the cell type abundance in our samples based on gene expression, we employed the CIBERSORT[81] computational deconvolution approach. A brain cell-type-specific gene signature was obtained from the Allen Brain Cell Atlas for mouse hippocampal single-cell reference at the class level (12 classes)[82], using the top 100 most differentially expressed genes per class as markers and capturing broad neuronal (glutamatergic and GABAergic) and non-neuronal (astrocyte and ependymal glia, oligodendrocyte lineage, vascular, and immune) populations. To apply this signature as the reference to our data, the mouse gene identifiers were mapped to their corresponding rat genes using the biomaRt Bioconductor package[83] with the Ensembl Genes database v115 annotation. The abundance of each member cell type was then estimated from the RNA-Seq data using the CIBERSOFT function from the IOBR 2.0 R package[84]. Differences in cell-type composition (fraction) across the samples were subsequently examined using the Kruskal-Wallis test, followed by Dunn's post-hoc test for pairwise comparisons.

Real-time PCR (RT-PCR)

To validate gene expression changes found in the RNA-seq analysis, the same RNA from that analysis was used to perform RT-PCR for specific genes of interest. For the conversion of RNA to cDNA, a standard protocol was followed using Promega reagents. Specifically, 1 µL of Oligo dT 15 primer (Promega) was added to 2 µg of RNA from each sample and incubated at 70 °C for 5 min to anneal the primer to the template. Samples were immediately placed on ice, and M-MLV reverse transcriptase (Promega) was added along with RNasin, dNTP mix, buffer, and enough water to bring the volume of the reaction mixture up to 25 µL. The mixture was incubated at 42 °C for 50 min to allow reverse transcription, then heated to 95 °C for 5 min to terminate the reaction.

Real-time PCR was carried out on an Applied Biosystems StepOne system. Power SYBR™ Green PCR Master Mix (Applied Biosystems) was combined with 150 ng cDNA and primers. The primers were designed to include only the exons. The procedure was done according to the manufacturer's instructions. Following pre-incubation at 94 °C for 15 min, PCR was performed for 40 cycles of denaturation, annealing, and elongation. Relative quantitation of gene expression was performed using GAPDH as an internal control. The $\Delta\Delta C_T$ method was used to compare the mRNA expression levels of each gene in experimental groups with control groups[85].

Data availability

The raw and processed RNA-Seq and RRBS data supporting the conclusions of this article are available in the NCBI Gene Expression Omnibus database (GEO Accession IDs: GSE287824 with the token for reviewer's access: mdujgyayplydlun). Analysis scripts used in the current study are freely available at our GitHub site (https://github.com/hurlab/EpilepsyEpigenetics). All other data generated or analyzed during this study are included in this article and its supplementary materials.

Received: 23 January 2025; Accepted: 8 January 2026
Published online: 13 January 2026

References

1. Fisher, R. S. et al. ILAE official report: a practical clinical definition of epilepsy. *Epilepsia* **55**, 475–482. https://doi.org/10.1111/epi.12550 (2014).
2. Hauser, W. A., Annegers, J. F. & Kurland, L. T. Prevalence of epilepsy in Rochester, minnesota: 1940–1980. *Epilepsia* **32**, 429–445 (1991).
3. Brodie, M. J. Antiepileptic drug therapy the story so Far. *Seizure* **19**, 650–655. https://doi.org/10.1016/j.seizure.2010.10.027 (2010).
4. Abou-Khalil, B. W. & Update on Antiseizure Medications. *Continuum (Minneap Minn)* 28, 500–535, (2022). https://doi.org/10.1212/CON.0000000000001104 (2022).
5. French, J. A. Refractory epilepsy: clinical overview. *Epilepsia* **48** (Suppl 1), 3–7. https://doi.org/10.1111/j.1528-1167.2007.00992.x (2007).
6. Mula, M. & Sander, J. W. Negative effects of antiepileptic drugs on mood in patients with epilepsy. *Drug Saf.* **30**, 555–567. https://doi.org/10.2165/00002018-200730070-00001 (2007).
7. Cramer, J. A., Mintzer, S., Wheless, J. & Mattson, R. H. Adverse effects of antiepileptic drugs: a brief overview of important issues. *Expert Rev. Neurother.* **10**, 885–891. https://doi.org/10.1586/ern.10.71 (2010).
8. French, J. A. et al. Antiepileptogenesis and disease modification: clinical and regulatory issues. *Epilepsia Open.* **6**, 483–492. https://doi.org/10.1002/epi4.12526 (2021).

9. Rho, J. M. & White, H. S. Brief history of anti-seizure drug development. *Epilepsia Open*. **3**, 114–119. https://doi.org/10.1002/epi4.12268 (2018).
10. Traynelis, S. F. et al. Epilepsy benchmarks area III: improved treatment options for controlling seizures and Epilepsy-Related conditions without side effects. *Epilepsy Curr.* **20**, 23S–30S. https://doi.org/10.1177/1535759719895279 (2020).
11. Binder, D. K. et al. Epilepsy benchmarks area II: prevent epilepsy and its progression. *Epilepsy Curr.* **20**, 14S–22S. https://doi.org/10.1177/1535759719895274 (2020).
12. Reddy, D. S. et al. Advances and challenges in experimental models of posttraumatic epilepsy for therapeutic interventions. *Pharmacol. Rev.* **77**, 100080. https://doi.org/10.1016/j.pharmr.2025.100080 (2025).
13. Kobow, K. & Blumcke, I. The emerging role of DNA methylation in epileptogenesis. *Epilepsia 53 Suppl.* **9**, 11–20. https://doi.org/10.1111/epi.12031 (2012).
14. Lubin, F. D. Epileptogenesis: can the science of epigenetics give Us answers? *Epilepsy Curr.* **12**, 105–110. https://doi.org/10.5698/1535-7511-12.3.105 (2012).
15. Younus, I. & Reddy, D. S. Epigenetic interventions for epileptogenesis: A new frontier for curing epilepsy. *Pharmacol. Ther.* **177**, 108–122. https://doi.org/10.1016/j.pharmthera.2017.03.002 (2017).
16. Boison, D. & Rho, J. M. Epigenetics and epilepsy prevention: the therapeutic potential of adenosine and metabolic therapies. *Neuropharmacology* **167**, 107741. https://doi.org/10.1016/j.neuropharm.2019.107741 (2020).
17. Berger, T. C. et al. Neuronal and glial DNA methylation and gene expression changes in early epileptogenesis. *PLoS One*. **14**, e0226575. https://doi.org/10.1371/journal.pone.0226575 (2019).
18. Vieira, A. S. et al. RNA sequencing reveals region-specific molecular mechanisms associated with epileptogenesis in a model of classical hippocampal sclerosis. *Sci. Rep.* **6**, 22416. https://doi.org/10.1038/srep22416 (2016).
19. Hansen, K. F., Sakamoto, K., Pelz, C., Impey, S. & Obrietan, K. Profiling status epilepticus-induced changes in hippocampal RNA expression using high-throughput RNA sequencing. *Sci. Rep.* **4**, 6930. https://doi.org/10.1038/srep06930 (2014).
20. Kobow, K. & Blumcke, I. The methylation hypothesis: do epigenetic chromatin modifications play a role in epileptogenesis? *Epilepsia* **52** (Suppl 4), 15–19. https://doi.org/10.1111/j.1528-1167.2011.03145.x (2011).
21. Kobow, K., El-Osta, A. & Blumcke, I. The methylation hypothesis of pharmacoresistance in epilepsy. *Epilepsia* **54** (Suppl 2), 41–47. https://doi.org/10.1111/epi.12183 (2013).
22. Kobow, K. et al. Increased reelin promoter methylation is associated with granule cell dispersion in human Temporal lobe epilepsy. *J. Neuropathol. Exp. Neurol.* **68**, 356–364. https://doi.org/10.1097/NEN.0b013e31819ba737 (2009).
23. Williams-Karnesky, R. L. et al. Epigenetic changes induced by adenosine augmentation therapy prevent epileptogenesis. *J. Clin. Inv.* **123**, 3552–3563 (2013).
24. Kobow, K. et al. Deep sequencing reveals increased DNA methylation in chronic rat epilepsy. *Acta Neuropathol.* **126**, 741–756. https://doi.org/10.1007/s00401-013-1168-8 (2013).
25. Miller-Delaney, S. F. et al. Differential DNA methylation profiles of coding and non-coding genes define hippocampal sclerosis in human Temporal lobe epilepsy. *Brain* **138**, 616–631. https://doi.org/10.1093/brain/awu373 (2015).
26. Miller-Delaney, S. F. et al. Differential DNA methylation patterns define status epilepticus and epileptic tolerance. *J. Neurosci.* **32**, 1577–1588. https://doi.org/10.1523/JNEUROSCI.5180-11.2012 (2012).
27. Bahabry, R. et al. Alterations in DNA 5-hydroxymethylation patterns in the hippocampus of an experimental model of chronic epilepsy. *Neurobiol. Dis.* **200**, 106638. https://doi.org/10.1016/j.nbd.2024.106638 (2024).
28. Bahabry, R. et al. Hippocampal gene expression changes associated with sequential behavioral training in a Temporal lobe epilepsy rat model. *Epilepsy Behav. Rep.* **29**, 100735. https://doi.org/10.1016/j.ebr.2024.100735 (2025).
29. Sint Jago, S. C. et al. Aerobic exercise alters DNA hydroxymethylation levels in an experimental rodent model of Temporal lobe epilepsy. *Epilepsy Behav. Rep.* **25**, 100642. https://doi.org/10.1016/j.ebr.2023.100642 (2024).
30. Pfisterer, U. et al. Identification of epilepsy-associated neuronal subtypes and gene expression underlying epileptogenesis. *Nat. Commun.* **11**, 5038. https://doi.org/10.1038/s41467-020-18752-7 (2020).
31. Kumar, P. et al. Single-cell transcriptomics and surface epitope detection in human brain epileptic lesions identifies pro-inflammatory signaling. *Nat. Neurosci.* **25**, 956–966. https://doi.org/10.1038/s41593-022-01095-5 (2022).
32. Racine, R. Kindling: the first decade. *Neurosurg* **3**, 234–252 (1978).
33. Boison, D., Scheurer, L., Tseng, J. L., Aebischer, P. & Mohler, H. Seizure suppression in kindled rats by intraventricular grafting of an adenosine releasing synthetic polymer. *Exp. Neurol.* **160**, 164–174 (1999).
34. Van Nieuwenhuyse, B. et al. The systemic Kainic acid rat model of Temporal lobe epilepsy: Long-term EEG monitoring. *Brain Res.* **1627**, 1–11. https://doi.org/10.1016/j.brainres.2015.08.016 (2015).
35. Vezzani, A. et al. Astrocytes in the initiation and progression of epilepsy. *Nat. Rev. Neurol.* **18**, 707–722. https://doi.org/10.1038/s41582-022-00727-5 (2022).
36. Gibbs, R. A. et al. Genome sequence of the brown Norway rat yields insights into mammalian evolution. *Nature* **428**, 493–521. https://doi.org/10.1038/nature02426 (2004).
37. Newman, A. M. et al. Robust enumeration of cell subsets from tissue expression profiles. *Nat. Methods*. **12**, 453–457. https://doi.org/10.1038/nmeth.3337 (2015).
38. Usui, T., Macleod, M. R., McCann, S. K., Senior, A. M. & Nakagawa, S. Meta-analysis of variation suggests that embracing variability improves both replicability and generalizability in preclinical research. *PLoS Biol.* **19**, e3001009. https://doi.org/10.1371/journal.pbio.3001009 (2021).
39. Witcher, K. G. et al. Comparison between midline and lateral fluid percussion injury in mice reveals prolonged but divergent cortical neuroinflammation. *Brain Res.* **1746**, 146987. https://doi.org/10.1016/j.brainres.2020.146987 (2020).
40. Ralay Ranaivo, H., Hodge, J. N., Choi, N. & Wainwright, M. S. Albumin induces upregulation of matrix metalloproteinase-9 in astrocytes via MAPK and reactive oxygen species-dependent pathways. *J. Neuroinflammation*. **9**, 68. https://doi.org/10.1186/1742-2094-9-68 (2012).
41. Kim, G. W. et al. The role of MMP-9 in integrin-mediated hippocampal cell death after pilocarpine-induced status epilepticus. *Neurobiol. Dis.* **36**, 169–180. https://doi.org/10.1016/j.nbd.2009.07.008 (2009).
42. Michaluk, P. et al. Influence of matrix metalloproteinase MMP-9 on dendritic spine morphology. *J. Cell. Sci.* **124**, 3369–3380. https://doi.org/10.1242/jcs.090852 (2011).
43. Nagy, V. et al. Matrix metalloproteinase-9 is required for hippocampal late-phase long-term potentiation and memory. *J. Neurosci.* **26**, 1923–1934. https://doi.org/10.1523/Jneurosci.4359-05.2006 (2006).
44. Chen, Z. et al. Increased microglial activation and astrogliosis after intranasal administration of Kainic acid in C57BL/6 mice. *J. Neurobiol.* **62**, 207–218. https://doi.org/10.1002/neu.20099 (2005).
45. Yan, B. C. et al. Changes in the Blood-Brain barrier function are associated with hippocampal neuron death in a Kainic acid mouse model of epilepsy. *Front. Neurol.* **9**, 775. https://doi.org/10.3389/fneur.2018.00775 (2018).
46. Oprica, M., Eriksson, C. & Schultzberg, M. Inflammatory mechanisms associated with brain damage induced by Kainic acid with special reference to the interleukin-1 system. *J. Cell. Mol. Med.* **7**, 127–140. https://doi.org/10.1111/j.1582-4934.2003.tb00211.x (2003).
47. Ehrencrona, E. et al. The IgGFc-binding protein FCGBP is secreted with all GDPH sequences cleaved but maintained by interfragment disulfide bonds. *J. Biol. Chem.* **297**, 100871. https://doi.org/10.1016/j.jbc.2021.100871 (2021).
48. Kobayashi, K., Hamada, Y., Blaser, M. J. & Brown, W. R. The molecular configuration and ultrastructural locations of an IgG Fc binding site in human colonic epithelium. *J. Immunol.* **146**, 68–74 (1991).

49. Vidarsson, G., Dekkers, G. & Rispens, T. IgG subclasses and allotypes: from structure to effector functions. *Front. Immunol.* **5**, 520. https://doi.org/10.3389/fimmu.2014.00520 (2014).
50. Michalak, Z. et al. IgG leakage May contribute to neuronal dysfunction in drug-refractory epilepsies with blood-brain barrier disruption. *J. Neuropathol. Exp. Neurol.* **71**, 826–838. https://doi.org/10.1097/NEN.0b013e31826809a6 (2012).
51. Reschke, C. R. et al. Systemic delivery of antagomirs during blood-brain barrier disruption is disease-modifying in experimental epilepsy. *Mol. Ther.* **29**, 2041–2052. https://doi.org/10.1016/j.ymthe.2021.02.021 (2021).
52. Albuz, B., Ozdemir, O. & Silan, F. The high frequency of chromosomal copy number variations and candidate genes in epilepsy patients. *Clin. Neurol. Neurosurg.* **202**, 106487. https://doi.org/10.1016/j.clineuro.2021.106487 (2021).
53. Kalozoumi, G. et al. Glial responses during epileptogenesis in Mus musculus point to potential therapeutic targets. *PLoS One.* **13**, e0201742. https://doi.org/10.1371/journal.pone.0201742 (2018).
54. Berger, T. C. et al. Differential glial activation in early Epileptogenesis-Insights from Cell-Specific analysis of DNA methylation and gene expression in the contralateral hippocampus. *Front. Neurol.* **11**, 573575. https://doi.org/10.3389/fneur.2020.573575 (2020).
55. Rousso-Noori, L. et al. Protein tyrosine phosphatase epsilon affects body weight by downregulating leptin signaling in a phosphorylation-dependent manner. *Cell. Metab.* **13**, 562–572. https://doi.org/10.1016/j.cmet.2011.02.017 (2011).
56. Moller, N. P. et al. Selective down-regulation of the insulin receptor signal by protein-tyrosine phosphatases alpha and epsilon. *J. Biol. Chem.* **270**, 23126–23131. https://doi.org/10.1074/jbc.270.39.23126 (1995).
57. Peretz, A. et al. Hypomyelination and increased activity of voltage-gated K(+) channels in mice lacking protein tyrosine phosphatase epsilon. *EMBO J.* **19**, 4036–4045. https://doi.org/10.1093/emboj/19.15.4036 (2000).
58. Liang, J., Shi, J., Wang, N., Zhao, H. & Sun, J. Tuning the protein phosphorylation by receptor type protein tyrosine phosphatase epsilon (PTPRE) in normal and cancer cells. *J. Cancer.* **10**, 105–111. https://doi.org/10.7150/jca.27633 (2019).
59. Ebner-Bennatan, S. et al. Multifaceted modulation of K + channels by protein-tyrosine phosphatase epsilon tunes neuronal excitability. *J. Biol. Chem.* **287**, 27614–27628. https://doi.org/10.1074/jbc.M112.342519 (2012).
60. Porter, N. M., Twyman, R. E., Uhler, M. D. & Macdonald, R. L. Cyclic AMP-dependent protein kinase decreases GABAA receptor current in mouse spinal neurons. *Neuron* **5**, 789–796. https://doi.org/10.1016/0896-6273(90)90338-g (1990).
61. Greengard, P., Jen, J., Nairn, A. C. & Stevens, C. F. Enhancement of the glutamate response by cAMP-dependent protein kinase in hippocampal neurons. *Science* **253**, 1135–1138. https://doi.org/10.1126/science.1716001 (1991).
62. Boulton, C. L., McCrohan, C. R. & O'Shaughnessy, C. T. Cyclic AMP analogues increase excitability and enhance epileptiform activity in rat neocortex in vitro. *Eur. J. Pharmacol.* **236**, 131–136 (1993).
63. Azevedo, H., Amato Khaled, N., Santos, P., Bernardi Bertonha, F. & Moreira-Filho, C. A. Temporal analysis of hippocampal CA3 gene coexpression networks in a rat model of febrile seizures. *Dis. Model. Mech.* **11** https://doi.org/10.1242/dmm.029074 (2018).
64. Corcoran, M. E., Kroes, R. A., Burgdorf, J. S. & Moskal, J. R. Regional changes in gene expression after limbic kindling. *Cell. Mol. Neurobiol.* **31**, 819–834. https://doi.org/10.1007/s10571-011-9672-7 (2011).
65. Wilcox, K. S., West, P. J. & Metcalf, C. S. The current approach of the epilepsy therapy screening program contract site for identifying improved therapies for the treatment of pharmacoresistant seizures in epilepsy. *Neuropharmacology* **166**, 107811. https://doi.org/10.1016/j.neuropharm.2019.107811 (2020).
66. Percie du Sert. The ARRIVE guidelines 2.0: updated guidelines for reporting animal research. *PLoS Biol.* **18**, e3000410. https://doi.org/10.1371/journal.pbio.3000410 (2020).
67. Racine Modification of seizure activity by electrical stimulation. II. Motor seizure. *Electroencephalogr. Clin. Neurophysiol.* **32**, 281–294 (1972).
68. Szybala, C. et al. Antiepileptic effects of silk-polymer based adenosine release in kindled rats. *Exp. Neurol.* **219**, 126–135. https://doi.org/10.1016/j.expneurol.2009.05.018 (2009).
69. Garrett-Bakelman, F. E. et al. Enhanced reduced representation bisulfite sequencing for assessment of DNA methylation at base pair resolution. *J. Vis. Exp.* **e52246** https://doi.org/10.3791/52246 (2015).
70. Bioinformatics, B. *FastQC: A quality control tool for high throughput sequence data.*, http://www.bioinformatics.babraham.ac.uk/projects/fastqc/ (.
71. Bolger, A. M., Lohse, M. & Usadel, B. Trimmomatic: a flexible trimmer for illumina sequence data. *Bioinformatics* **30**, 2114–2120. https://doi.org/10.1093/bioinformatics/btu170 (2014).
72. Bioinformatics, B. *Trim Galore!* https://www.bioinformatics.babraham.ac.uk/projects/trim_galore/ (.
73. Kim, D., Langmead, B. & Salzberg, S. L. HISAT: a fast spliced aligner with low memory requirements. *Nat. Methods.* **12**, 357–360. https://doi.org/10.1038/nmeth.3317 (2015).
74. Liao, Y., Smyth, G. K. & Shi, W. FeatureCounts: an efficient general purpose program for assigning sequence reads to genomic features. *Bioinformatics* **30**, 923–930. https://doi.org/10.1093/bioinformatics/btt656 (2014).
75. Love, M. I., Huber, W. & Anders, S. Moderated Estimation of fold change and dispersion for RNA-seq data with DESeq2. *Genome Biol.* **15**, 550. https://doi.org/10.1186/s13059-014-0550-8 (2014).
76. Krueger, F. & Andrews, S. R. Bismark: a flexible aligner and methylation caller for Bisulfite-Seq applications. *Bioinf. (Oxford England).* **27**, 1571–1572. https://doi.org/10.1093/bioinformatics/btr167 (2011).
77. Langmead, B. & Salzberg, S. L. Fast gapped-read alignment with bowtie 2. *Nat. Methods.* **9**, 357–359. https://doi.org/10.1038/nmeth.1923 (2012).
78. Akalin, A. et al. MethylKit: a comprehensive R package for the analysis of genome-wide DNA methylation profiles. *Genome Biol.* **13** (R87). https://doi.org/10.1186/gb-2012-13-10-r87 (2012).
79. Akalin, A., Franke, V., Vlahovicek, K., Mason, C. E. & Schubeler, D. Genomation: a toolkit to summarize, annotate and visualize genomic intervals. *Bioinformatics* **31**, 1127–1129. https://doi.org/10.1093/bioinformatics/btu775 (2015).
80. Zerbino, D. R. et al. Ensembl. *Nucleic Acids Res* 46, D754-D761, (2018). https://doi.org/10.1093/nar/gkx1098 (2018).
81. Newman, A. M. et al. Determining cell type abundance and expression from bulk tissues with digital cytometry. *Nat. Biotechnol.* **37**, 773–782. https://doi.org/10.1038/s41587-019-0114-2 (2019).
82. Yao, Z. et al. A high-resolution transcriptomic and Spatial atlas of cell types in the whole mouse brain. *Nature* **624**, 317–332. https://doi.org/10.1038/s41586-023-06812-z (2023).
83. Durinck, S. et al. BioMart and bioconductor: a powerful link between biological databases and microarray data analysis. *Bioinformatics* **21**, 3439–3440. https://doi.org/10.1093/bioinformatics/bti525 (2005).
84. Zeng, D. et al. Enhancing immuno-oncology investigations through multidimensional decoding of tumor microenvironment with IOBR 2.0. *Cell. Rep. Methods.* **4**, 100910. https://doi.org/10.1016/j.crmeth.2024.100910 (2024).
85. Livak, K. J. & Schmittgen, T. D. Analysis of relative gene expression data using real-time quantitative PCR and the 2(-Delta Delta C(T)) Method. *Methods* 25, 402–408, (2001). https://doi.org/10.1006/meth.2001.1262
86. Ashburner, M. et al. Gene ontology: tool for the unification of biology. *Nat. Genet.* **25**, 25–29 (2000). doi:Doi 10.1038/75556.
87. Kanehisa, M. & Goto, S. K. E. G. G. Kyoto encyclopedia of genes and genomes. *Nucleic Acids Res.* **28**, 27–30. https://doi.org/10.1093/nar/28.1.27 (2000).
88. Huang, D. W. et al. The DAVID Gene Functional Classification Tool: a novel biological module-centric algorithm to functionally analyze large gene lists. *Genome Biol* 8, R183, (2007). https://doi.org/10.1186/gb-2007-8-9-r183

Author contributions

DR, SM, JG, and DB contributed to the design and conception of the work. BP, JH, DR, MM, FT, RS, and NR

contributed to the acquisition and analysis of the data. BP, JH, MM, SM, JG, and DB contributed to the interpretation of the data and the drafting of the manuscript and its revisions.

Funding
This study was funded through grants NS127846 (DB), NS065957 (DB, SM, JG), K99NS140499 (BP) and F32NS117792 (BP).

Declarations

Competing interests
DB is co-founder and CDO of PrevEp Inc. All other authors have no interests to declare.

Additional information
Supplementary Information The online version contains supplementary material available at https://doi.org/10.1038/s41598-026-35826-6.

Correspondence and requests for materials should be addressed to D.B.

Reprints and permissions information is available at www.nature.com/reprints.

Publisher's note Springer Nature remains neutral with regard to jurisdictional claims in published maps and institutional affiliations.